Resorbable Glass-Ceramic Phosphate-Based Scaffolds for Bone Tissue Engineering: Synthesis, Properties and *In Vitro* Effects on Human Marrow Stromal Cells

CHIARA VITALE-BROVARONE,[1,*] GABRIELA CIAPETTI,[2] ELISA LEONARDI,[2] NICOLA BALDINI,[2] OANA BRETCANU,[1] ENRICA VERNÉ[1] AND FRANCESCO BAINO[1]

[1]*Materials Science and Chemical Engineering Department, Politecnico di Torino, Corso Duca degli Abruzzi 24, 10129 Torino, Italy*

[2]*Laboratorio di Fisiopatologia Ortopedica e Medicina Rigenerativa, Istituto Ortopedico Rizzoli, Via di Barbiano 1/10, 40136 Bologna, Italy*

* Corresponding author: Chiara Vitale-Brovarone

E-mail: chiara.vitale@polito.it

Tel.: +39 011 564 4716

Fax: +39 011 564 4699

ABSTRACT: Highly porous bioresorbable glass-ceramic scaffolds were prepared via sponge replication method by using an open-cells polyurethane foam as a template and phosphate-based glass powders. The glass, belonging to the P_2O_5-SiO_2-CaO-MgO-Na_2O-K_2O system, was synthesized by a melting-quenching route, ground and sieved to obtain powders below 30 μm. A slurry containing glass powders, polyvinyl alcohol and water was prepared to coat the polymeric template. The removal of the polymer and the sintering of the glass powders were performed by a thermal treatment, in order to obtain an inorganic replica of the template structure. Scaffold structure and properties were investigated from structural, morphological and mechanical viewpoints by means of X-ray diffraction, scanning electron microscopy, density measurements, image analysis and compressive tests. The scaffolds exhibited a trabecular architecture that closely mimics the structure of natural spongy bone. The solubility of the porous structures was assessed by soaking the samples in acellular simulated body fluid (SBF) and Tris-HCl for different time frames and then by assessing the scaffold weight loss. As far as the test in SBF is concerned, the nucleation of hydroxyapatite on scaffold trabeculae demonstrates the bioactivity of the material. Biological tests were carried out using human bone marrow stromal cells to test the osteoconductivity of the material. The cells adhered to the scaffold struts and were metabolically active; it was found that cell differentiation over proliferation occurred. Therefore, the produced scaffolds, being biocompatible, bioactive, resorbable and structurally similar to spongy bone, can be proposed as interesting candidates for bone grafting.

KEY WORDS: Scaffold; Phosphate glass; Glass-ceramic; Bone marrow cells; Bone graft.

INTRODUCTION

Natural bone is a composite material with extraordinary properties of self-remodelling in reply to external mechanical stresses. Bone is also the human tissue, after the blood, with the highest demand for reconstruction and substitution [1] due to tumours [2], trauma [3] or various bone diseases [4]. Synthetic bone grafts have attracted the interest of the researchers in order to overcome the traditional limitations of autografts and allografts, such as patient/donor pain and infection [5], limited availability, immune rejection and diseases transfer risk [6].

3-D bone scaffolds should fulfil a series of requirements in order to promote the osteointegration of the implant and the growth of newly formed bone [7]. First of all, the scaffold must be biocompatible and should be recognized as "self" by the organism. Moreover, the scaffold has the purpose to reproduce the morphology of natural bone, because its structure will conduct the regenerating tissue. Specifically, the shape of the regenerated tissue must match the original tissue architecture in 3-D. The main scaffold purposes are (i) to provide a temporary support in the bone defect region while the natural tissue regenerates, (ii) to guarantee the growth of newly formed bone inside the implant and (iii) to allow the inclusion of cells, proteins or growth factors accelerating the tissue regeneration process. The fulfilment of all these requirements is not trivial, because some of them are in contrast with one another. For example, on one hand the scaffold should possess a highly interconnected porous structure to allow a proper vascularisation of the implant, but on the other hand the mechanical strength of the implant decreases with the increase of porosity. Many studies were carried out to state the optimal features of a synthetic scaffold for bone substitution. A macroporosity of 100-500 μm is needed to favour bone cell attachment [8], a microporosity of less than 10 μm should promote protein adhesion and oxygen/ion/nutrient diffusion within the implant [9] and a total porosity within 50-70% vol. is desirable to reproduce the structure of cancellous bone [10].

Over the last four decades, various types of ceramic materials have been proposed for scaffolding, e.g. hydroxyapatite (HA), β-tricalcium phosphate (β-TCP), HA/β-TCP composites and several bioactive glasses and glass-ceramics. As regards the glass-derived scaffolds for bone tissue engineering, most researches has been focused on SiO_2-based materials. However, in the last years the use of phosphate glasses and glass-ceramics has attracted increasing attention for tissue engineering applications [11], as they undergo a controllable degradation with a resorption rate that matches bone healing and cells regeneration rate. In addition, as the implant is temporary, no foreign substance is left in the patient body, thus reducing the inflammation risk [12].

P_2O_5-based glasses resemble the structure of polymers and their solubility is due to phosphate chains cleavage and ions release [13-14]. Vogel et al. prepared resorbable glass-ceramics belonging to the system P_2O_5-CaO-Na_2O with some Al_2O_3 content to control the dissolution rate [15]. Uo et al. studied the cytotoxicity of P_2O_5-CaO-Na_2O glasses upon dissolution in water or simulated body fluid [13]. More recently, it was demonstrated that the degradation rate of phosphate glasses can be tailored by adding metal oxides, such as TiO_2 [16-17], CuO [18] and Fe_2O_3 [19-20] to the glass composition.

The purpose of this study was to fabricate and characterize resorbable highly porous glass-derived scaffolds, obtained *via* sponge replication method [21-22] by using a polyurethane (PU) foam as a sacrificial template and a P_2O_5-based bioactive glass. The scaffolds were investigated from structural, morphological and mechanical viewpoints; their solubility in two different media, i.e. Tris-HCl and SBF, was also tested, and finally the response of human marrow stromal cells (hMSCs) cultured on the scaffolds was analyzed.

MATERIALS AND METHODS

Synthesis of starting glass

The starting glass, belonging to the P_2O_5-SiO_2-CaO-MgO-Na_2O-K_2O system (ICEL) [23-24], had the following molar composition: 45% P_2O_5, 3% SiO_2, 26% CaO, 7% MgO, 15% Na_2O, 4% K_2O. ICEL was prepared by melting the high-purity raw products (Sigma-Aldrich), i.e. $(NH_4)_2HPO_4$, SiO_2, $Ca_3(PO_4)_2$, $Mg_3(PO_4)_2 \cdot 8H_2O$, $Na_3PO_4 \cdot 12H_2O$ and K_2HPO_4, in a platinum crucible at 1200 °C for 1 h in air (heating rate set at 10 °C·min^{-1}) and by pouring the melt onto a preheated stainless steel plate to produce bars, that were subsequently ground by ball milling. Specifically, a six-ball zirconia mill was used for grinding the glass; compositional analyses carried out on the so-obtained glass powder demonstrated that no contamination occurred during the milling process. The glass particles were finally sieved to a final grain size below 30 μm.

Scaffolds fabrication

ICEL-derived scaffolds were produced by using a sacrificial organic template and ICEL powders. The chosen organic template was a commercial PU sponge (apparent density: ~20 kg·m^{-3}) with an open and interconnected macroporosity. The sponge was cut into 15 mm × 15 mm × 15 mm cubic blocks and then impregnated with a water-based ICEL slurry that was prepared by dispersing the glass powders into distilled water; polyvinyl alcohol (PVA, Sigma-Aldrich) was also used as a binder in order to control the slurry viscosity and to optimize the ability of glass particles to firmly adhere to the sponge. The chosen weight ratio of the slurry components was 35% ICEL, 6% PVA, and 59% water. First PVA was hydrolyzed and stirred in distilled water at 60 °C for 1 h, and then the glass powders were dispersed in the solution. Afterwards, the porous sponge underwent the infiltration process. The sponge blocks were soaked for 30 s into the prepared ICEL slurry that

infiltrated the polymer structure thereby coating its surfaces with the glass particles. The exceeding slurry was squeezed out by shrinking the impregnated sponge up to 60% in thickness along the three spatial directions.

After the infiltration process, the samples were dried at room temperature for 6 h and thermally treated at 610 °C for 3 h (heating and cooling rate set at 5 and 10 °C·min^{-1} respectively) in order to (i) remove the polymer template and (ii) sinter the glass particles. The sintering conditions were set on the basis of the hot stage microscopy carried out on the ICEL glass sample and reported elsewhere [24].

Structural, morphological and mechanical characterization of the scaffolds

ICEL-derived scaffolds were ground in powders and analyzed by means of wide-angle (2θ within 10-70°) X-ray diffraction (XRD; X'Pert Philips diffractometer: working conditions 40 kV and 30 mA, Bragg Brentano camera geometry, Cu anode Kα incident radiation with wavelength λ = 1.5405 Å) to assess the presence of crystalline phases nucleated during the thermal treatment.

The morphology of the scaffolds was qualitatively studied through scanning electron microscopy (SEM Philips 525 M equipped with EDAX Philips 9100 for compositional analysis) in order to observe the effectiveness of the sintering treatment and to evaluate the pores size and their geometry, distribution and interconnection degree. The samples were silver-coated and observed at an accelerating voltage of 15 kV.

By means of geometrical mass-volume measurements performed on 15 cubic 10 mm × 10 mm × 10 mm samples, the total pore content Π (%vol.) of the scaffolds was assessed as

$$\Pi = \left(1 - \frac{\rho_s}{\rho_g}\right) \times 100 \quad (1)$$

where ρ_s is the scaffold apparent density (mass/volume ratio) and ρ_g is the bulk ICEL density.

A quantitative evaluation of the pores size distribution and amount was attained through image analysis studies (Qwin Leica software) on low-magnification SEM images of polished scaffolds cross-sections.

Volume shrinkage measurements were carried out on five ICEL-derived scaffolds. The volumetric shrinkage Σ (%), due to PU foam removal and to ICEL particles softening and sintering, was evaluated as

$$\Sigma = \left(1 - \frac{V_s}{V_0}\right) \times 100 , \tag{2}$$

where V_s is the scaffold final volume and V_0 is the volume of the impregnated sponge.

The strength of the scaffolds was evaluated through crushing tests on 10 mm × 10 mm × 10 mm cubic samples (MTS System Corp. apparatus, cross-head speed set at 1 mm·min^{-1}). The compressive failure stress σ_c (MPa) was calculated as

$$\sigma_c = \frac{L_M}{A_R} , \tag{3}$$

being L_M (N) the maximum load registered during the test and A_R (mm^2) the resistant section area; five scaffolds were tested to obtain an average failure stress.

The energy per unit volume E_V (J·mm^{-3}) absorbed by the scaffold till the breaking off is reached was defined as the energy necessary to deform a specimen from the unloaded condition to the failure strain ε_f , and was calculated as the area under the stress-strain curve up to ε_f [25]:

$$E_V = \int_0^{\varepsilon_f} \sigma(\varepsilon) d\varepsilon , \tag{4}$$

where the strain ε is the integration variable ; the initial condition is $\sigma(\varepsilon = 0) = 0$ and the final state is $\sigma(\varepsilon = \varepsilon_f) = \sigma_c$ (calculated from Eq.(3)).

Solubility tests

Solubility tests were carried out on the scaffolds in order to evaluate the erosion rate and the dissolution kinetics of the samples. The tests were carried out according to ISO standard [26] by soaking the scaffolds in 25 ml of Tris-HCl and acellular simulated body fluid (SBF) maintained at 37 °C for different time frames. SBF, prepared according to Kokubo's protocol [27], is the standard to simulate acellular body plasma. Both media were replaced every 48 h to simulate fluid circulation in the human body. Scaffold solubility was quantitatively estimated by assessing the weight loss after 7 days and 1, 2, 3 months of soaking. After soaking, the samples were extracted from the solution, dried at room temperature for 24 h and finally weighed. The weight losses were calculated in two ways, as Λ_w (%) and Λ_S (g·cm^{-2}), according to the following formulas:

$$\Lambda_w = \left(1 - \frac{w_s}{w_0}\right) \times 100 \tag{5}$$

$$\Lambda_S = \frac{w_0 - w_s}{S} \tag{6}$$

where w_0 and w_s are, respectively, the scaffold weights before and after soaking and S (cm^2) is the scaffold external surface exposed to the solutions.

The tests were performed on triplicate samples, and the presented weight losses are an average of the acquired data. During sample soaking, daily evaluations of the solutions pH were carried out to assess pH variations due to ion-leaching phenomena.

Biological tests

Sample preparation

The samples (~10 mm^3 cubic scaffolds) were weighed, in dry conditions, before and after cell culture, to assess their eventual weight loss during *in vitro* testing. Sterilization was obtained by soaking the samples in 70% ethanol (2 h) and in 1% antibiotic/antimycotic (2 h). A dynamic pre-

wetting step in 10% serum-added medium (1 h) was performed to facilitate sample conditioning and to improve cell adhesion.

Cell isolation and expansion

hMSCs were isolated from bone marrow tissue during total hip replacement surgery. The study was approved by the Institutional Ethical Committee, and a written consent was obtained from all patients. Mononuclear cells (MNCs), collected according to a standard protocol already adopted in previous studies [28], were plated in polystyrene flasks and incubated with α-Minimum Essential Medium (α-MEM), 10% fetal bovine serum, 2 mM glutamine and 1% penicillin/streptomycin (basal medium) at 37 °C in 5% CO_2, and non-adherent cells were removed after 4 days. Adherent hMSCs were cultured in basal medium added with 50 $\mu g \cdot ml^{-1}$ ascorbate-2 phosphate and splitted at subconfluence. Second passage cells were used for the experiments on ICEL-derived scaffolds.

Cell seeding and culture

Cells were seeded at a density of 10^5 cells/scaffold by applying 30 µl of cell suspension on the samples at 37°C for 30 min in a wet chamber via "droplet technique", which is useful to avoid that cells slip down from the top of the scaffold to attach to bottom culture dish; afterwards, 1.5 ml of medium was added to cover samples. To improve cell migration into the scaffold, cultures were maintained in dynamic conditions for the first 24 h. hMSCs seeded at 4×10^4 cells/well in 24-well (well diameter: 15.6 mm) tissue culture plastic plates (TCPS) provided the controls.

Seeding efficiency was calculated 1 day after plating, by comparing the DNA values from Picogreen test to a reference curve; it should be underlined that 24 h after seeding the scaffolds with cells were transferred to another 24-well plate, to avoid any interference with biochemical assays due to the cells at the bottom.

Cells were fed twice a week with an osteogenic medium, i.e. basal medium plus 10^{-8} M dexamethasone. At 1, 7, 14 and 21 days morphological and biochemical assays were performed on cell-seeded samples and controls.

Morphological assays

Cell morphology of hMSCs on scaffolds was monitored by light microscopy throughout the culture period. Ultrastructural analysis was carried out by SEM at the final time endpoint by properly processing the cell-seeded samples as described elsewhere [29].

Biochemical assays

The pH of the supernatant in cell-seeded scaffolds was measured 3 times a week by using colorimetric stripes (range 6.0-8.0, Merck).

Alamar Blue test (Biosource International-CA) was used to asses cell viability; fluorescence was measured using a CytoFluor 2350 plate reader (Millipore Corporation, Bedford, MA, USA) with 490/530 nm of excitation/emission wavelengths. Results were expressed as Relative Fluorescence Units (RFU).

DNA content was quantified by Picogreen assay (Quant-IT Picogreen dsDNA, Invitrogen): after cells lysis with 0.01% SDS and sonication; fluorescence was read at 480-520 nm.

Alkaline phosphatase (ALP) activity was measured by a chromogenic assay involving the conversion of p-nitrophenyl phosphate substrate to p-nitrophenol. The absorption was measured at 405 nm with a spectrophotometer (Spectra III, Tecan, Austria), and phosphatase activity calculated using a calibration curve by serial dilution of p-nitrophenol standard solution. ALP activity was normalized to total protein content, used as an index of cell number.

Levels of C-terminal propeptide of type I collagen (CICP), released in the supernatant, were quantified by enzyme immunoassay according to the manufacturer's instructions (Quidel corporation, Heidelberg, Germany).

Statistics

Results are reported as mean ± standard error of three separate experiments on duplicate samples and controls. Differences were assessed using non-parametric analysis of variance (Kruskal-Wallis test); Mann–Whitney test was performed as a *post hoc* test of the multiple analyses, or as unpaired comparison for 2 independent variables. The level of statistical significance was established at $p < 0.05$.

RESULTS AND DISCUSSION

Scaffolds structure and morphology

ICEL is a bioresorbable phosphate-based glass developed by modifying the chemical composition of a bioactive but not bioresorbable silicate glass (CEL2) previously proposed and investigated by the authors [30]. Specifically, the molar amounts of SiO_2 and P_2O_5 in the ICEL composition are inverted in comparison with those of CEL2. The presence of SiO_2, as reported by other authors [31], is useful to increase the degradation rate of the phosphate glass. In addition, it was demonstrated that silicon ions can stimulate gene expression of osteoblasts in order to induce bone mineralization [32-33]. The features of glassy ICEL and ICEL-derived bulk glass-ceramic samples (GC-ICEL) was described and discussed elsewhere in detail [24,28].

Figure 1(a) reports the XRD pattern of as-poured ICEL: the presence of a broad halo demonstrates that the material does not contain crystalline phases and it is an amorphous glass, as reported elsewhere [24]. The sintering treatment induces the nucleation and growth of two crystalline phases,

that were identified as $Na_2Mg(PO_4)_3$ (sodium/magnesium phosphate) and $Ca_2P_2O_7$ (calcium pyrophosphate), in good accordance with a previous work [28]; therefore, the resulting scaffolds are glass-ceramic (GC-ICEL). The main peaks assigned to these two phases are marked in the XRD pattern of Figure 1(b). Calcium pyrophosphate is well known to be biocompatible and to act as HA precursor [28,34].

Figure 2(a) shows the morphology of the commercial PU sponge used as a template for the ICEL-derived scaffolds. The polymeric sponge was coated with a thin layer of ICEL slurry in order to obtain a glass-ceramic replica of the organic template after the burning-out of the organic phase. The results of the sponge impregnation process can be observed in Figures 2(b) and 2(c). Pore size ranges from 100 up to 1000 μm, and the thickness of the trabeculae is within 20-80 μm. The size and amount of ICEL particles and the presence of a binder (PVA) are the parameters that mainly influence the slurry viscosity. The slurry features were chosen to avoid the presence of clotted pores and to obtain an uniform and homogeneous coating of ICEL particles on the sponge trabeculae also in the inner part of the template.

The morphology of the resulting GC-ICEL scaffold can be observed in Figure 2(d); details of the scaffold surface and cross-section are reported in Figures 3(a) and 3(b), respectively. As expected, the structure of the PU sponge was substituted by a sintered scaffold with similar texture; therefore, inorganic replicas of the PU template were finally obtained. The pores are open and highly interconnected also in the inner part of the scaffold, as shown in Figure 3(b); in addition, the pores are homogeneously distributed along the scaffold cross-section. The obtained glass-ceramic scaffolds are characterized by an open and interconnected network of macropores ranging within 50-600 μm (Figure 2(b) and Figure 3) and a diffused microporosity (below 50 μm) on scaffold struts and pore walls (Figure 4(a)). The densification of the pores struts confirms that a good degree of sintering was achieved, as it is impossible to distinguish the original glass particles.

As shown in Figure 4(a), the thickness of pore struts is about few tens of microns and the trabecular structure closely mimics that of the natural cancellous bone. By comparing Figure 2(c) with Figure

4(a), it is evident that the sintered trabeculae of GC-ICEL scaffolds are thinner than the struts of the impregnated sponge, due to PU removal and ICEL particles densification during sintering. Figure 4(b) puts into evidence the glass-ceramic nature of ICEL-derived scaffolds, as previously assessed by XRD investigations. A diffuse struts roughness, due to the presence of crystalline phases, is clearly distinguishable. This is an important feature, because it is known that proteins adhesion and cell spreading are promoted by a rough surface [35-37].

Porosity analysis

The volumetric shrinkage of the scaffolds after the thermal treatment was $\Sigma = 46.6 \pm 3.0$ % and the total porosity was $\Pi = 81.0 \pm 1.1$ %vol.; it should be noticed that a very low standard deviation was observed confirming that the adopted method for scaffolding leads to reproducible samples.

The pore size and distribution were investigated on polished sections of GC-ICEL scaffolds by means of image analysis using the Qwin Program of Leica. The input for the program analysis was a series of SEM micrographs depicting scaffold cross-sections, in which the black-white contrast was emphasized to highlight the pores. Then a measure frame was selected on the image and used to evaluate the pore amount and distribution. The pores are supposed to be approximately circular by the software; hence, the equivalent diameter D (μm) is calculated as $D = 2\sqrt{A/\pi}$, where A (μm^2) is the actual pore area. The darker areas in the processed images are pores that will be identified by the program as empty spaces.

A number of measure frames were randomly selected, so that the results are an average of the data acquired from different cross-sections. Firstly the whole pore range (0-600 μm) was considered for the analysis, and then the pores with an equivalent diameter lower than 50 μm (microporosity) were omitted in order to consider only the macropores contribution; the results are summarized in Table 1.

The acquired data are further processed to obtain two bar charts showing the pore amount and the pore area *versus* the pore equivalent diameter. An example of this analysis is depicted in Figure 5. Macropores above 100 μm are crucial for the vascularization of the implant: Figure 5(b) shows that the highest contribution to the whole pore area is given by pores of size within 100-600 μm. Specifically, ~95% of the total pore area consists of pores above 100 μm, and thus large enough to allow blood vessels and cells migration inside the scaffold *in vivo*.

Scaffold mechanical properties

The compressive strength of the scaffolds was $\sigma_c = 0.4 \pm 0.3$ MPa; an example of stress-strain curve is shown in Figure 6. The curve exhibits a peak followed by a stress drop; the saw-toothed profile of the curve is due to the progressive cracking of scaffold trabeculae and this behaviour is typical for brittle ceramics, as described elsewhere [22]. The energy absorption capacity was calculated from the area under the stress-strain curve; specifically, the energy absorbed by the scaffold up to its breaking off was $E_V = (2.0 \pm 1.0)\times10^{-5}$ J·mm^{-3}. This value is comparable – as order of magnitude – to that found by other authors for hydroxyapatite scaffolds [38].

The mechanical strength of GC-ICEL scaffolds is comparable to that exhibited by Bioglass®-derived glass-ceramic scaffolds with similar porosity [39], which, at present, are commonly considered the standard reference for highly porous glass-derived scaffolds. However, it can not be ignored that the strength of GC-ICEL scaffolds is one order of magnitude lower than that of spongy bone, due to the presence of a very high number of pores that reduce the sample resistant section. Nonetheless, this strength values is sufficient for the scaffolds to be handled, cut (as shown in Figure 3(b)) and/or manipulated for the solubility tests. In addition, it has been underlined by other authors that the compressive strength of a scaffold can significantly increase *in vivo* due to tissue in-growth [40]. In fact, the cells on the scaffold, the newly formed tissue and the scaffold itself can create an in situ biocomposite, increasing the scaffold strength with time [7].

Solubility tests

Solubility tests were carried out on GC-ICEL scaffolds by soaking the samples in SBF and Tris-HCl. The soaking in SBF is the more relevant test because the solution is known to closely simulate the human plasma and thus the environment in which the scaffolds would be implanted.

In Figure 7(a) a high-magnification SEM image of the scaffold surface after soaking for 7 days in SBF can be observed. A diffused microporosity (pore size < 10 μm), constituted by pores similar to small pits, is clearly distinguishable. In addition, globular agglomerates (< 5 μm) of a newly formed phase are also visible on pores boundaries. Such agglomerates revealed to be rich in calcium and phosphorous, as qualitatively shown by the compositional analysis reported in the inset of Figure 7(a); the peaks corresponding to silver are due to the sample metal coating. These observations demonstrate that, during soaking in SBF, two mechanisms took place at the same time: (i) scaffold dissolution and (ii) precipitation of calcium phosphates on the scaffold surface. Therefore, GC-ICEL scaffolds are not only resorbable, as expected, but also bioactive according to the mechanism described by Hench for some particular glasses and glass-ceramics [41]. The presence of an apatite-like layer, able to mimic the hydroxycarbonate apatite of bone mineral, is crucial to promote the formation of a stable interface between scaffold surface and host living bone. In addition, it was demonstrated that the osteoblasts adhere, spread, proliferate and produce new bone preferably on an apatite-coated surface according to the well-known mechanism of osteoconduction [35,37].

Figure 7(b) depicts the scaffold structure after soaking for 7 days in Tris-HCl. No precipitation of new phases occurs, but the scaffold undergoes a fast process of congruent erosion: its struts become progressively thinner and the pore size increases. However, the scaffold maintains its structural integrity.

The erosion of the scaffolds after soaking in both SBF and Tris-HCl is confirmed by the image analysis data reported in Table 2. By comparing these data with those shown in Table 1, it is clearly

evident that an enlargement of the scaffold pores occurred. Pores within 600-1000 μm, not found in the scaffolds before soaking, were seen in the samples soaked for 3 months in the two solutions.

The weight losses after soaking in Tris-HCl and SBF are reported in Figure 8. These results are consistent with the data of image analysis (Table 2): the erosion of the scaffold inner walls caused a significant increase of the average pore diameter, i.e. from ~30% for the samples in SBF up to ~80% for those in Tris-HCl. As expected, the weight loss for the scaffolds in Tris-HCl is higher than those of the samples in SBF, confirming what was previously discussed about SEM observations, and putting into evidence that GC-ICEL scaffold dissolution rate is strongly dependent on the medium in which the scaffold is soaked. In addition, the dissolution rate is also time-dependent, as it seems that the major dissolution occurs, both in Tris-HCl and in SBF, during the first month of soaking.

In a previous work the solubility of ICEL-derived glass-ceramic bulk samples (GC-ICEL) in Tris-HCl and SBF was studied and discussed in detail [28]. As expected, the weight losses of GC-ICEL scaffolds are significantly higher than those of GC-ICEL bulk samples, as the scaffolds are characterized by a larger surface area. In fact, the effective surface area useful for ion-exchange with the solutions includes both the exposed outer surface (*S*) of the scaffold and the scaffold inner trabecular surfaces, that were put into contact with the fluids because of the high degree of pore interconnection.

The pH changes occurring in Tris-HCl and SBF, induced by the scaffold dissolution, range within 7.25-7.55, and are very moderate in both solutions in comparison with the initial pH value of 7.40.

Biological tests

GC-ICEL scaffold/medium interactions

The pH of the culture medium was measured to verify if ions released by GC-ICEL scaffold can change optimal culture conditions. It has been found that the pH in hMSC-seeded samples was

always lower than in control cultures, but the values, ranging between 6.3 and 7.2 during the 3 week-culture period, did not negatively affect the viability and growth of the cells (Figure 9).

The seeding efficiency on GC-ICEL scaffolds was (33.9 ± 7.9)%.

At 3 weeks of culture, GC-ICEL scaffolds had lost up to 25% of the initial weight. The majority of this loss (15%) occurred in the first 24 h after cell seeding. A few considerations on this point are necessary. The weight losses occurring during the biological tests were recorded and reported for purpose of completeness, but it should be underlined that the culture medium, essentially constituted by α-MEM and foetal bovine serum, is not the fluid commonly adopted for assessing samples solubility. The solubility tests were previously carried out by soaking the scaffolds in SBF and Tris-HCl (Figure 8) according to the procedure outlined by international standards [26]. The discrepancy between the weight losses reported in Figure 8 and those derived from immersion in the culture medium can be due to the different test conditions: in fact, during culture the scaffold was gently agitated for 24 h to improve cell entrance within the scaffold pores (dynamic conditions), and this may have caused some additional material loss.

Cell viability and proliferation

The viability of hMSCs grown on GC-ICEL scaffolds was good. GC-ICEL scaffolds did not alter the metabolic activity of hMSCs, that increased progressively along the whole culture time period (Figure 10(a)). The values on TCPS were higher than on GC-ICEL scaffold surfaces at each time point.

The DNA content of control cells became higher over culture time, as well. On the contrary, DNA of hMSCs on samples decreased during the first 14 days and then slightly increased at 21 days (Figure 10(b)). Difference between TCPS and GC-ICEL scaffolds was statistically significant at all time points.

In order to explain the contrast between the results of the viability test and the DNA content, two hypotheses can be assumed. The first explanation (Hp1) moves from the consideration that a

remarkable GC-ICEL scaffold degradation, with some ion release in the culture medium, occurs during the cellular tests. This could induce the detachment of metabolically active cells from the scaffold, causing an underestimation of the actual DNA content. Scaffold degradation could be emphasized by test dynamic conditions, that caused displacement of cells with material fragments in the supernatant. An unfavourable effect of phosphate-based glass surfaces on cell adhesion has been found also by other authors using human bone marrow stromal cells and human fetal osteoblast 1.19 cells [42]. On the contrary, the second hypothesis (Hp2) moves from biological/biochemical considerations. As it will be described later, hMSCs cultured on GC-ICEL scaffolds produce type I collagen, whose amount progressively increased along the culture period. Collagen provides the main structural component of extracellular matrix (ECM), which restricts cell proliferation to stimulate differentiation. In such a condition, hMSCs remain metabolically active, thus converting Alamar blue to formazan deposits, but most of the quiescent cells are entrapped within ECM and cannot be easily removed from the surface. As a consequence of these effects, DNA measured in the cell lysate is reduced at the final endpoint.

The ultrastructural details of GC-ICEL scaffold with cultured cells were observed by using SEM (Figure 11). Cells were elongated and firmly attached to glass asperities through cytoplasmic prolongations. They were not homogeneously distributed on the scaffolds, but rather grew in clusters; this behaviour of the cells is consistent with that observed for hMSCs cultured on GC-ICEL slices [28]. A progressive increase with time to cell confluence was not observed, suggesting that cell proliferation reached a plateau at the time points analysed.

Osteogenic differentiation

The alkaline phosphatase activity, marker of early osteogenic differentiation, was not significantly modified along the culture period in control cells, whereas hMSCs grown on GC-ICEL scaffolds showed a steadily increasing ALP production (Figure 12(a)). hMSCs cultured on GC-ICEL scaffolds were able to produce type I collagen, too, and the amount increased progressively with

time. Likewise, cells grown on TCPS showed a similar behaviour, with a statistically significant increase from 24 h to 7 days (Figure 12(b)).

Collagen and ALP production confirm that hMSCs cultured on GC-ICEL scaffolds go toward osteogenic differentiation. An enhanced collagen release by rat osteoblast-like cells on bioactive glasses was found by other authors, too [43]. Specifically, a stimulation of hMSC differentiation over proliferation occurred, as previously mentioned, although the ALP increase seems to indicate that differentiation was not complete but an ongoing process at the time points analyzed.

CONCLUSIONS

In this research, glass-ceramic scaffolds were produced by the sponge impregnation method, using a polyurethane template as pore former and bioresorbable phosphate-based glass powders. Scaffolds characterized by open and highly interconnected macropores, with a trabecular morphology analogous to the texture of cancellous bone, were obtained. A total pore content above 80% vol., including macropores (50-600 μm) and micropores (below 50 μm), was achieved.

The scaffolds showed to be resorbable as, after soaking in media simulating the biological fluids, they underwent a process of continuous dissolution, whose rate was both medium and time dependent. In fact, it was assessed that the major dissolution occurs during the first month of soaking. Morphological and biochemical assays with human marrow-derived stromal cells seeded on GC-ICEL scaffolds showed that hMSCs maintain their metabolic activity and ability to proliferate on the scaffolds, but differentiation over proliferation occurred, thereby suggesting potential osteogenic properties of the scaffold material.

Therefore, the proposed scaffolds are resorbable, bioactive – as hydroxyapatite was found on scaffold trabeculae after soaking in SBF –, osteoconductive and might have a stimulatory effect in promoting osteogenesis.

ACKNOWLEDGEMENTS

Regione Piemonte (Ricerca Sanitaria Finalizzata 2006 and 2008) and the IntraEuropean Marie Curie fellowship (BIORESS) are kindly acknowledged for supporting this research work.

REFERENCES

1. Service, R.F. (2000). Tissue Engineers Build New Bone, *Science*, **289**: 1498-1500.
2. Yamamoto, T., Onga, T., Marui, T. and Mizuno, K. (2000). Use of Hydroxyapatite to Fill Cavities after Excision of Benign Bone Tumours: Clinical Results, *J. Bone Joint Surg. Br.*, **82**: 1117-1120.
3. Hinz, P., Wolf, E., Schwesinger, G., Hartelt, E. and Ekkernkamp, A. (2002). A New Resorbable Bone Void Filler in Trauma: Early Clinical Experience and Histologic Evaluation, *Orthopedics*, **25**: 597-600.
4. Meadow G.R. (2002). Adjunctive Use of Ultraporous Beta-Tricalcium Phosphate Bone Void Filler in Spinal Arthrodesis, *Orthopedics*, **25**: 579-584.
5. Younger, E.M. and Chapman, M.W. (1989). Morbidity at Bone Graft Donor Site, *J. Orthop. Trauma*, **3**: 192-195.
6. Hutmacher, D.W. (2000). Scaffolds in Tissue Engineering Bone and Cartilage, *Biomaterials*, **21**: 2529-2543.
7. Jones, J.R. and Hench, L.L. (2003). Regeneration of Trabecular Bone Using Porous Ceramics, *Curr. Opin. Solid State Mater. Sci.*, **7**: 301-307.
8. De Aza, P.N., Luklinska, Z.B., Santos, C., Guitian, F. and De Aza, S. (2003). Mechanism of Bone-Like Formation on a Bioactive Implant In Vivo, *Biomaterials*, **24**: 1437-1445.

9. Rokusek, D., Davitt, C., Bandyopadhyay, A., Bose, S. and Hosick, H.L. (2005). Interaction of Human Osteoblasts with Bioinert and Bioactive Ceramic Substrates, *J. Biomed. Mater. Res. A*, **75**: 588-594.
10. Le Huec, J., Schaeverbeke, T., Clement, D., Faber, J. and Le Rebeller, A. (1995). Influence of Porosity on the Mechanical Resistance of Hydroxyapatite Ceramics under Compressive Stress, *Biomaterials*, **16**: 113-118.
11. Hench, L.L. (1998). Biomaterials: A Forecast for the Future, *Biomaterials*, **19**: 1419-1423.
12. Middleton, J.C. and Tipton, A.J. (2000). Synthetic Biodegradable Polymers as Orthopaedic Devices, *Biomaterials*, **21**: 2335-2346.
13. Uo, M., Mizuno, M., Kuboki, Y., Makishima, A. and Watari, F. (1998). Properties and Cytotoxicity of Water Soluble Na_2O-CaO-P_2O_5 Glasses, *Biomaterials*, **19**: 2277-2284.
14. Bitar, M., Salih, V., Mudera, V., Knowles, J.C. and Lewis, M.P. (2004). Soluble Phosphate Glasses: *In Vitro* Studies Using Human Cells of Hard and Soft Tissue Origin, *Biomaterials*, **25**: 2283-2292.
15. Vogel, W. and Holand, W. (1987). Development of Bioglass Ceramics for Medical Applications, *Angew. Chem. Int. Ed.*, **26**: 527-544.
16. Abou Neel, E.A., Mizoguchi, T., Ito, M., Bitar, M., Salih, V. and Knowles, J.C. (2007). In Vitro Bioactivity and Gene Expression by Cells Cultured on Titanium Dioxide Doped Phosphate-Based Glasses, *Biomaterials*, **28**: 2967-2977.
17. Abou Neel, E.A. and Knowles, J.C. (2008). Physical and Biocompatibility Studies of Novel Titanium Dioxide Doped Phosphate-Based Glasses for Bone Tissue Engineering Applications, *J. Mater. Sci: Mater. Med.*, **19**: 377-386.
18. Abou Neel, E.A., Ahmed, I., Pratten, J., Nazhat, S.N. and Knowles, J.C. (2005). Characterisation of Antibacterial Copper Releasing Degradable Phosphate Glass Fibres, *Biomaterials*, **26**: 2247-2254.

19. Ahmed, I., Collins, C.A., Lewis, M.P., Olsen, I. and Knowles, J.C. (2004). Processing, Characterisation and Biocompatibility of Iron-Phosphate Glass Fibres for Tissue Engineering, *Biomaterials*, **25**: 3223-3232.
20. Abou Neel, E.A., Ahmed, I., Blaker, J.J., Bismarck, A., Boccaccini, A.R., Lewis, M.P., Nazhat, S.N. and Knowles, J.C. (2005). Effect of Iron on the Surface, Degradation and Ion Release Properties of Phosphate-Based Glass Fibres, *Acta Biomater.*, **1**: 553-563.
21. Vitale-Brovarone, C., Verné, E., Robiglio, L., Appendino, P., Bassi, F., Martinasso, G., Muzio, G. and Canuto, R. (2007). Development of Glass-Ceramic Scaffolds for Bone Tissue Engineering: Characterisation, Proliferation of Human Osteoblasts and Nodule Formation, *Acta Biomater.*, **3**: 199-208.
22. Vitale-Brovarone, C., Baino, F. and Verné, E. (2009). High Strength Bioactive Glass-Ceramic Scaffolds for Bone Regeneration, *J. Mater. Sci.: Mater. Med.*, **20**: 643-653.
23. Vitale-Brovarone, C., Verné, E., Baino, F., Ciapetti, G., Leonardi, E. and Baldini, N. (2008). Bioresorbable Phosphate Scaffolds for Bone Regeneration, *Key Eng. Mater.*, **361-363**: 241-244.
24. Vitale-Brovarone, C., Baino, F., Bretcanu, O. and Verné, E. (2009). Foam-Like Scaffolds for Bone Tissue Engineering Based on a Novel Couple of Silicate-Phosphate Specular Glasses: Synthesis and Properties, *J. Mater. Sci: Mater. Med.*, **20**: 2197-2205.
25. Kenesei, P., Kadar, C., Rajkovits, Z. and Lendvai, J. (2004). The Influence of Cell-Size Distribution on the Plastic Deformation in Metal Foams, *Scripta Mater.*, **50**: 295-300.
26. ISO 10993-14:2002 standard. Biological evaluation of medical devices: identification and quantification of degradation products from ceramics.
27. Kokubo, T. and Takadama, H. (2006). How Useful is SBF in Predicting *In Vivo* Bone Bioactivity?, *Biomaterials*, **27**: 2907-2915.

28. Leonardi, E., Ciapetti, G., Baldini, N., Novajra, G., Verné, E., Baino, F. and Vitale-Brovarone, C. (2010). Response of Human Bone Marrow Stromal Cells to a Novel Phosphate Glass-Ceramic for Tissue Engineering Applications, *Acta Biomater.*, **6**: 598-606.
29. Causa, F., Netti, P.A., Ambrosio, L., Ciapetti, G., Baldini, N., Pagani, S., Martini, D. and Giunti, A. (2006). Poly-epsilon-caprolactone/Hydroxyapatite Composites for Bone Regeneration: *In Vitro* Characterization and Human Osteoblast Response, *J. Biomed. Mater. Res. A*, **76**: 151-162.
30. Vitale-Brovarone, C., Verné, E., Robiglio, L., Martinasso, G., Canuto, R.A. and Muzio, G. (2008). Biocompatible Glass-Ceramic Materials for Bone Substitution, *J. Mater. Sci: Mater. Med.*, **19**: 471-478.
31. Patel, A. and Knowles, J.C. (2006). Investigation of Silica-Iron-Phosphates Glasses for Tissue Engineering, *J. Mater. Sci.: Mater. Med.*, **17**: 937-944.
32. Xynos, I.D., Edgar, A.J., Buttery, L.D.K., Hench, L.L. and Polak, J.M. (2000). Ionic Products of Bioactive Glass Dissolution Increase Proliferation of Human Osteoblasts and Induce Insulin-Like Growth Factor II mRNA Expression and Protein Synthesis, *Biochem. Biophys. Res. Commun.*, **276**: 461-465.
33. Hench, L.L., Polak, J.M., Xynos, I.D. and Buttery, L.D.K. (2000). Bioactive Materials to Control Cell Cycle, *Mater. Res. Innov.*, **3**: 313-323.
34. Cao, W. and Hench, L.L. (1996). Bioactive Materials, *Ceram. Int.*, **22**: 493-507.
35. Schwartz, Z. and Boyan, B.D. (1994). Characterization of Microrough Bioactive Glasses: Surface Reactions and Osteoblast Responses, *J. Cell. Biochem.*, **56**: 340-347.
36. Schwartz, Z., Hummert, T.W., Cochran, D.L., Simpson, J., Dean, D.D. and Boyan, B.D. (1996). Surface Roughness Modulates the Local Production of Growth Factors and Cytokines by Osteoblast-Like MG-63 Cells, *J. Biomed. Mater. Res.*, **32**: 55-63.
37. Boyan, B.D., Hummert, T.W., Dean, D.D. and Schwartz, Z. (1996). Role of Material Surfaces in Regulating Bone and Cartilage Cell Response, *Biomaterials*, **17**: 137-146.

38. Kim, H.W., Knowles, J.C. and Kim, H.E. (2005). Hydroxyapatite Porous Scaffolds Engineered with Biological Polymer Hybrid Coating for Antibiotic Vancomycin Release, *J. Mater. Sci.: Mater. Med.*, **16**; 189-195.

39. Chen, Q.Z., Thompson, I.D. and Boccaccini, A.R. (2006). 45S5 Bioglass®-Derived Glass-Ceramic Scaffolds for Bone Tissue Engineering, *Biomaterials*, **27**: 2424-2425.

40. Tamai, N., Myoui, A., Tomita, T., Nakase, T., Tanaka, J. and Ochi, T. (2002). Novel Hydroxyapatite Ceramics with an Interconnective Porous Structure Inhibit Superior Osteoconduction In Vivo, *J. Biomed. Mater. Res.*, **59**: 110-117.

41. Hench, L.L., Splinter, R.J., Allen, W.C. and Greenlee, T.K. (1972). Bonding Mechanism at the Interface of Ceramic Prosthetic Materials, *J. Biomed. Mater. Res.*, **2**: 117-141.

42. Skelton, K.L., Glenn, J.V., Clarke, S.A., Georgiu, G., Valappil, S.P., Knowles, J.C., Nazhat, S.N. and Jordan, G.R. (2007). Effect of Ternary Phosphate-Based Glass Compositions on Osteoblast and Osteoblast-Like Proliferation, Differentiation and Death *In Vitro*, *Acta Biomater.*, **3**: 563-572.

43. Bosetti, M., Zanardi, L., Hench, L.L. and Cannas, M. (2003). Type I Collagen Production by Osteoblast-Like Cells Cultured in Contact with Different Bioactive Glasses, *J. Biomed. Mater. Res. A*, **64**: 189-195.

Tables

Table 1. Average pore diameter of as-done GC-ICEL scaffolds obtained via image analysis.

Size range	Average diameter (μm)
All pores (0-600 μm)	~18.0 [a]
Macropores (50-600 μm)	155.0 ± 2.0

[a] The standard deviation was omitted due to high pore size dispersion.

Table 2. Average pore diameter of GC-ICEL scaffolds after soaking for 3 months in SBF and Tris-HCl.

Size range	Soaking medium	Average diameter (μm)
All pores (0-1000 μm)	SBF	~25.0 [b]
Macropores (50-1000 μm)		200.0 ± 4.0
All pores (0-1000 μm)	Tris-HCl	~30.0 [b]
Macropores (50-1000 μm)		270.0 ± 9.0

[b] The standard deviation was omitted due to high pore size dispersion.

Figure

Figure 1. XRD pattern of (a) as-poured ICEL and (b) ICEL-derived scaffold ground in powders.

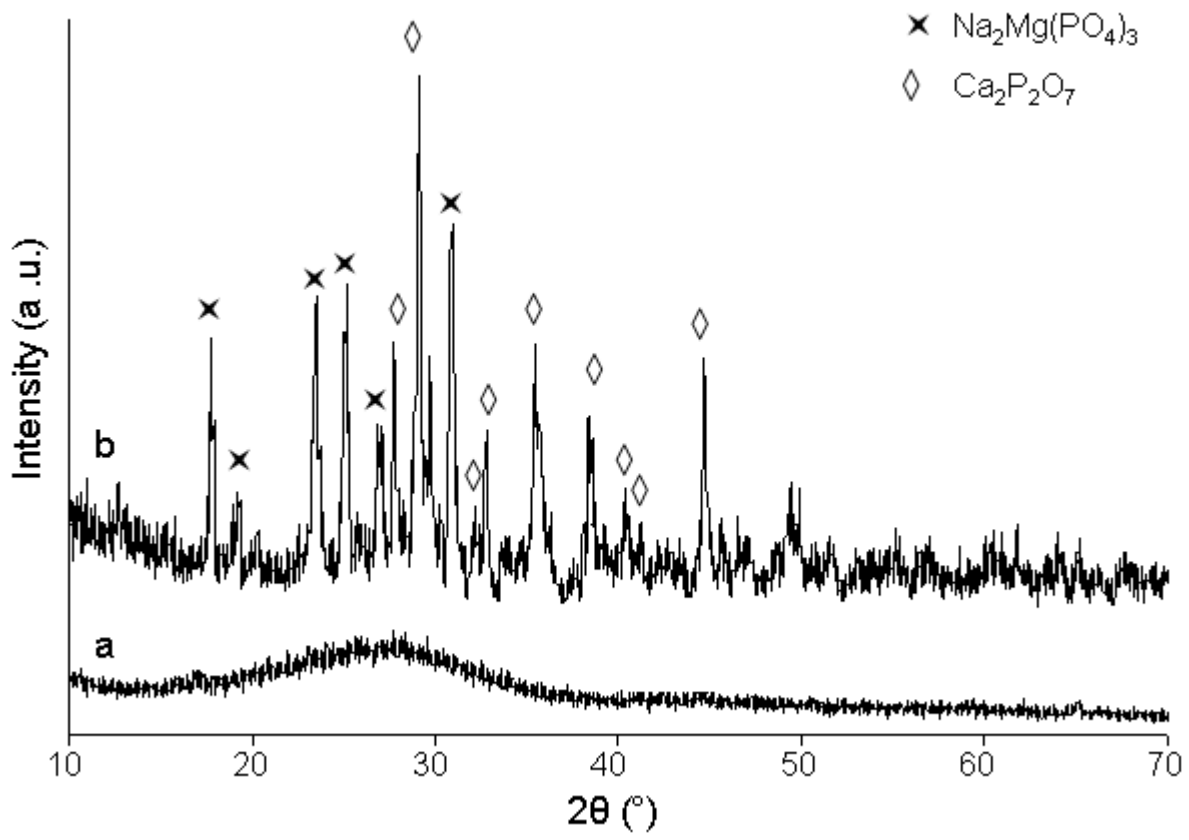

Figure 2. Scaffold preparation: (a) bare polymeric template; (b)-(c) impregnated sponge at different magnifications; (d) ICEL scaffold structure.

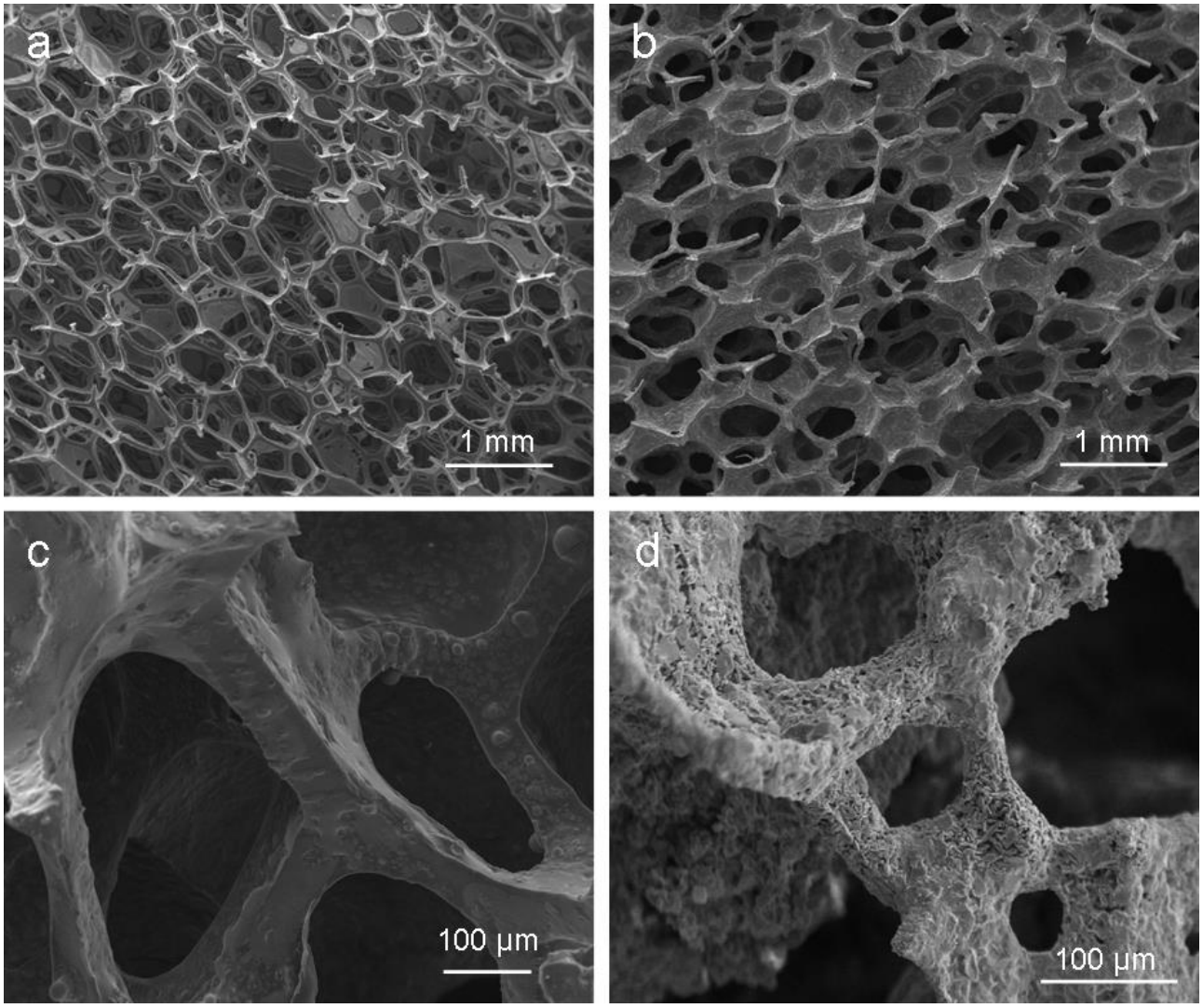

Figure 3. Scaffold morphology: (a) surface; (b) cross-section.

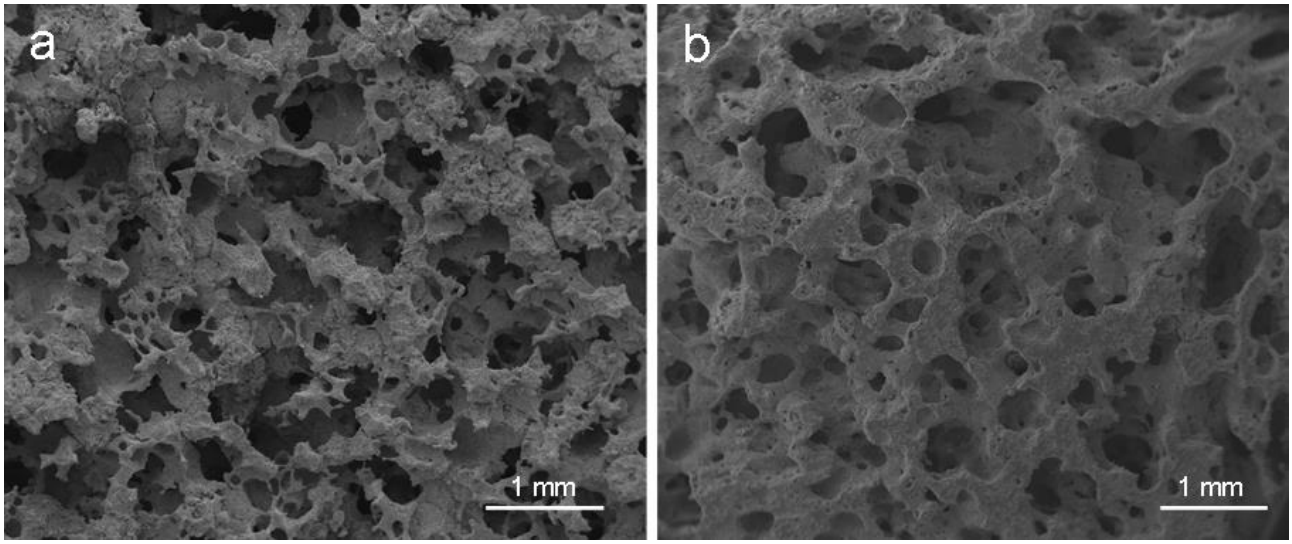

Figure 4. Scaffold structure at different magnifications: (a) trabecular texture; (b) crystals on scaffold struts.

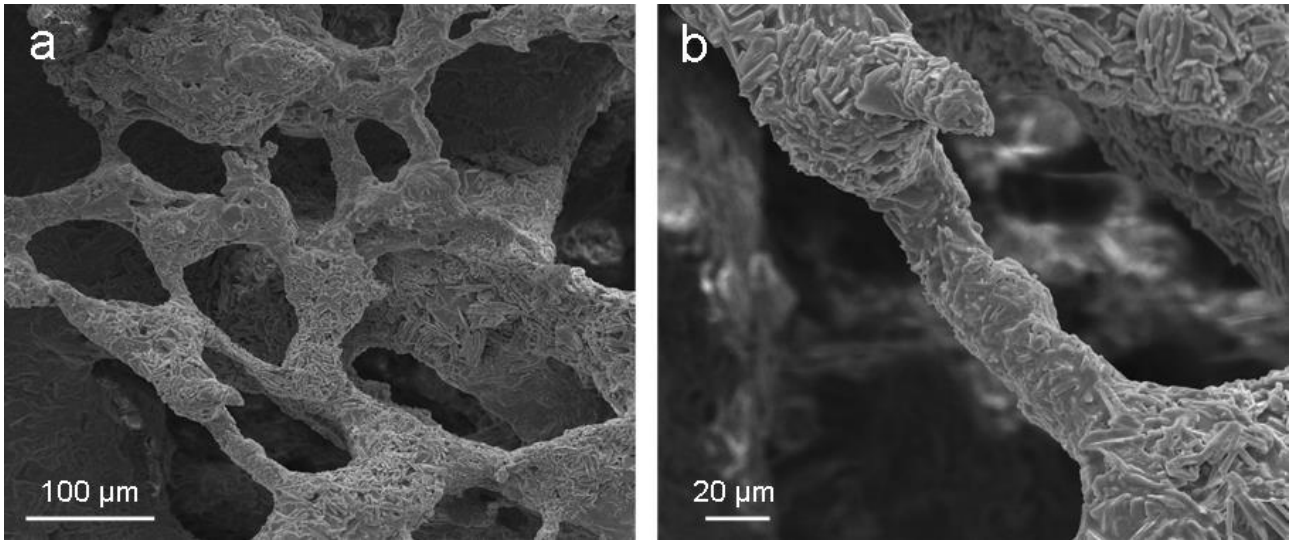

Figure 5. Histograms showing image analysis results on GC-ICEL scaffolds: (a) pores amount and (b) pores area depending from the equivalent diameter.

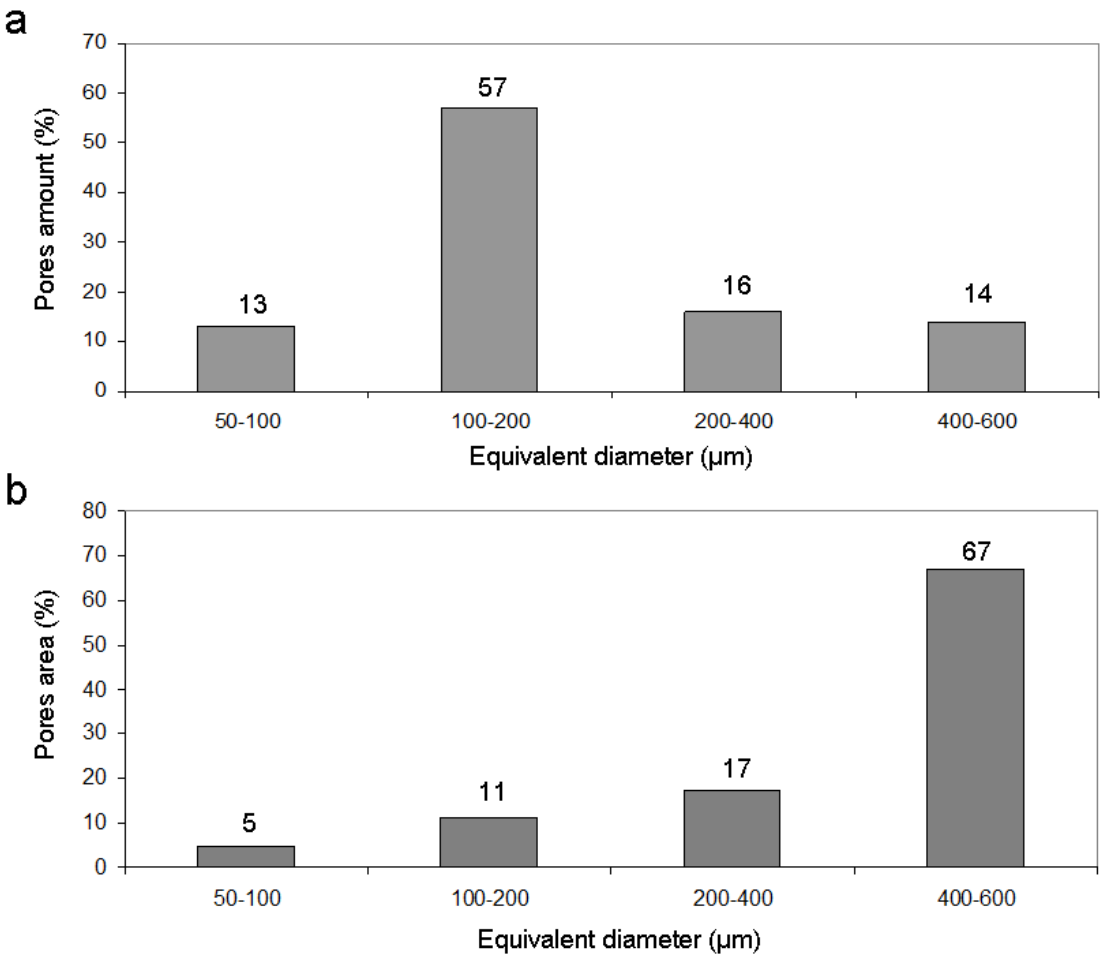

Figure 6. Stress-strain curve typical for GC-ICEL scaffolds.

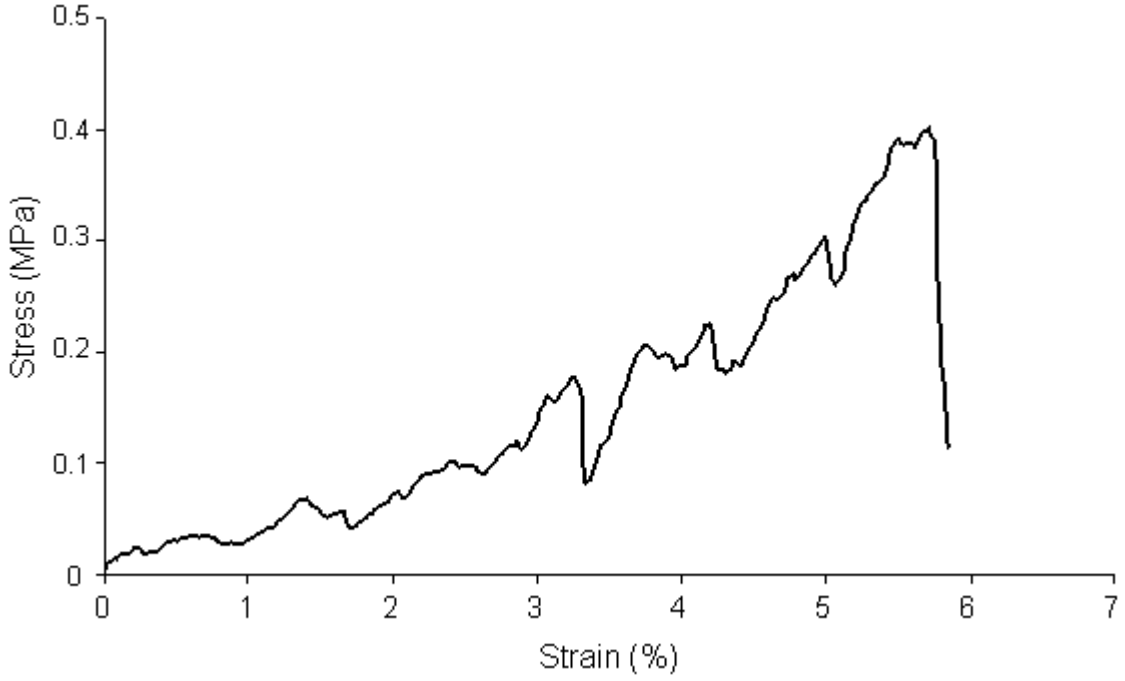

Figure 7. Scaffold after soaking for 7 days in (a) SBF (inset: compositional analysis on the newly formed globular agglomerates, some of which emphasized in white circles) and (b) Tris-HCl.

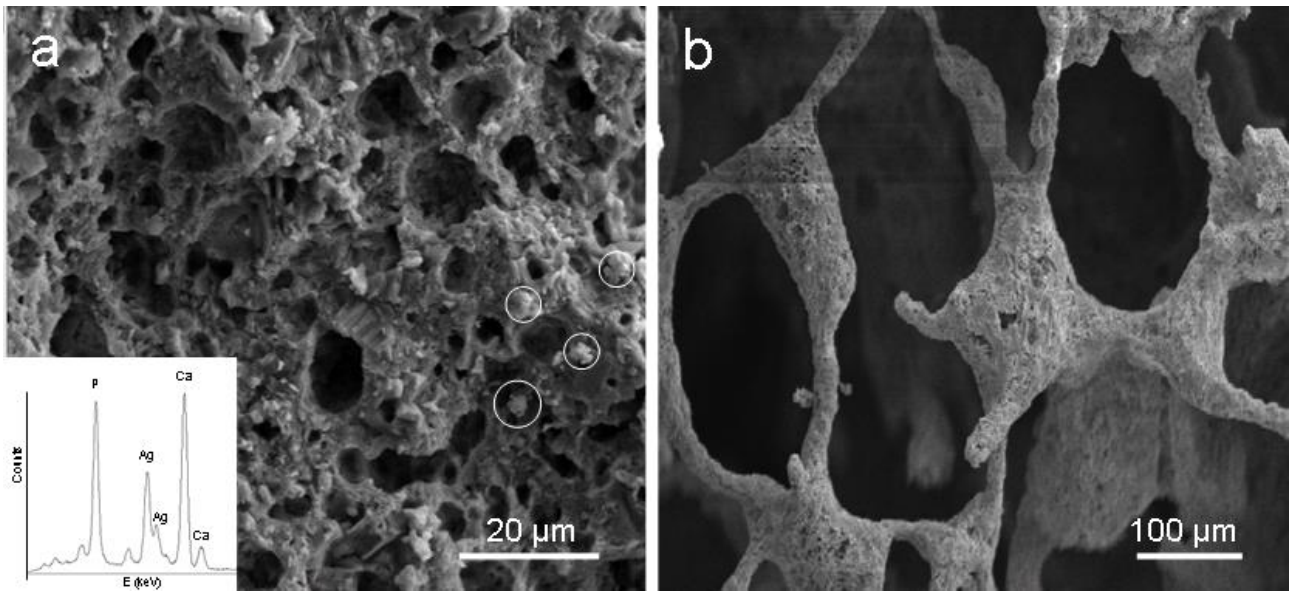

Figure 8. Quantitative analysis of scaffolds solubility (weight loss) of GC-ICEL scaffold after soaking in SBF and Tris-HCl.

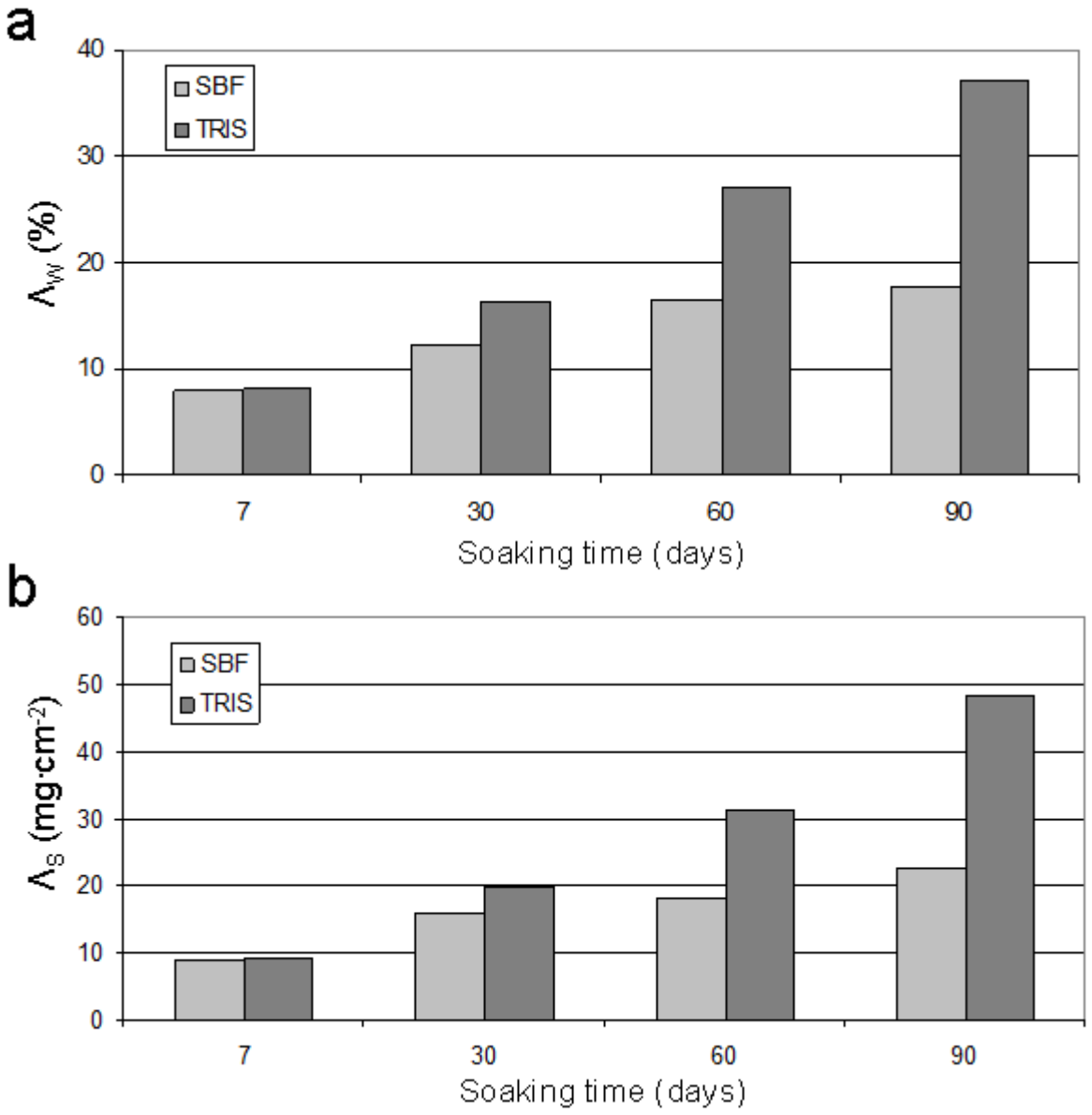

Figure 9. Variations of medium pH during the culture period of hMSCs on GC-ICEL scaffolds (S-GC-ICEL) and TCPS.

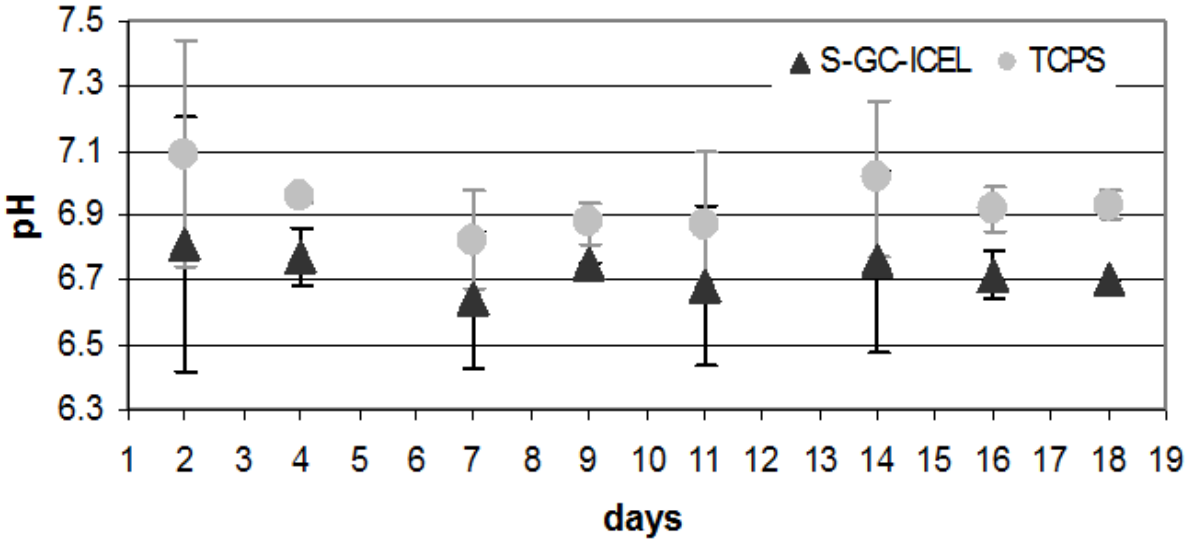

Figure 10. Effect of GC-ICEL scaffolds (S-GC-ICEL) on hMSC viability and proliferation measured by Alamar (a) and Picogreen (b) assays at 1, 7, 14 and 21 days. Results are displayed in graphs respectively with linear (Alamar) and logarithmic (Picogreen) scale. * $p < 0.05$ in TCPS 7 days *vs* 1day (a) and in both TCPS and S-GC-ICEL 7 days *vs* 1 day, 14 days *vs* 7 days (b).

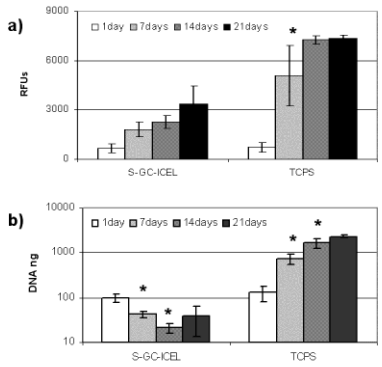

Figure 11. SEM analysis of hMSCs on GC-ICEL scaffolds at 7 (a,b), 14 (c,d) and 21 days (e,f) of cell culture. White bars correspond to 100 µm (a,c,e) or 10 µm (b,d,f).

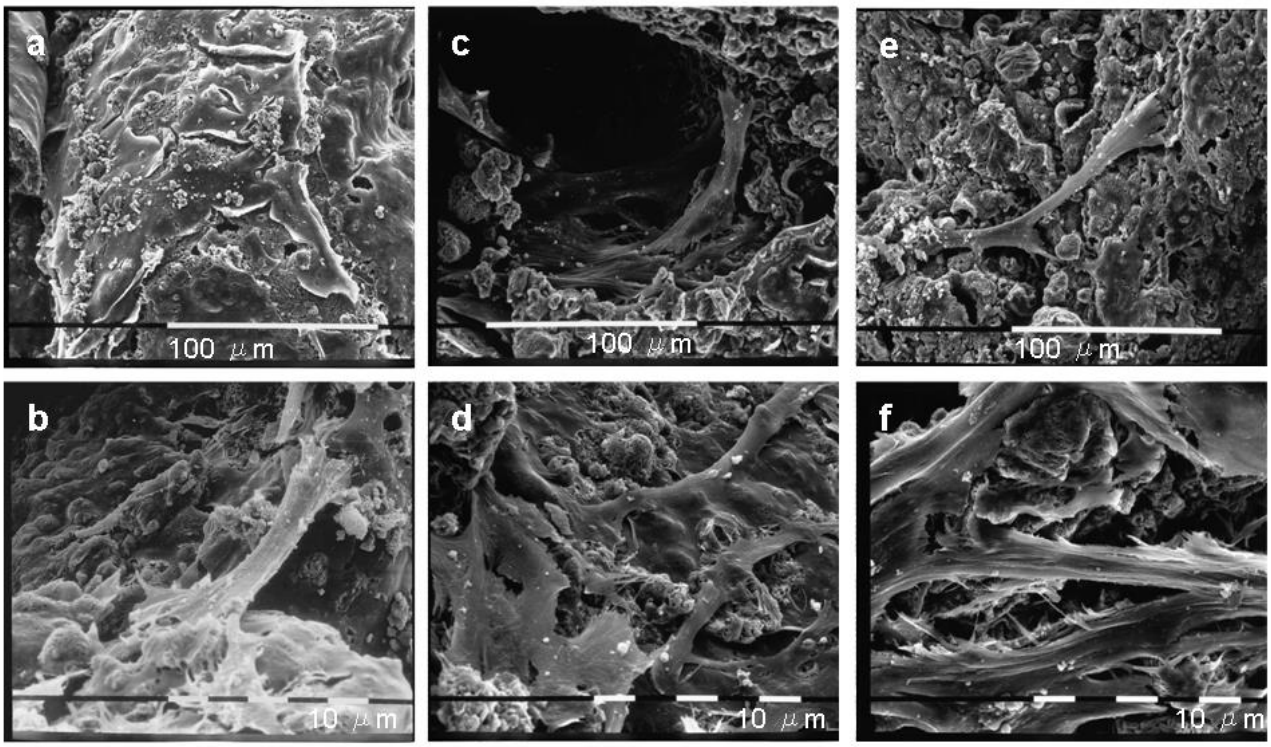

Figure 12. Effect of GC-ICEL scaffold (S-GC-ICEL) on hMSC osteogenic differentiation markers: alkaline phosphatase activity from lysate (a) and collagen release in the culture supernatant (b) were quantified at 1, 7, 14 and 21 days. * $p < 0.05$ in both TCPS and S-GC-ICEL 7 days *vs* 1 day, 14 days *vs* 7 days (b).